Surface & Coatings Technology 309 (2017) 911–919

Contents lists available at ScienceDirect

Surface & Coatings Technology

journal homepage: www.elsevier.com/locate/surfcoat

Wear and corrosion properties of HVOF coatings from Superduplex alloy modified with addition of boron

José Eduardo Berger [a,*], Robert Schulz [b], Sylvio Savoie [b], Juno Gallego [c], Claudio Shyinti Kiminami [a], Claudemiro Bolfarini [a], Walter José Botta [a]

[a] Federal University of São Carlos, Department of Materials Engineering, Rod. Washington Luiz km. 235, 13565–905 São Carlos, SP, Brazil
[b] Hydro-Quebec Research Institute, 1800 boul, Lionel Boulet, Varennes, (QC) J3X 1S1, Canada
[c] Department of Mechanical Engineering, UNESP, Avenida Brasil, 56, 15385–000 Ilha Solteira, SP, Brazil

ARTICLE INFO

Article history:
Received 5 July 2016
Revised 18 October 2016
Accepted in revised form 23 October 2016
Available online 25 October 2016

Keywords:
High-velocity oxygen fuel (HVOF)
Superduplex alloy
Partially amorphous structure
Nanocrystalline borides
Abrasive wear resistance
Corrosion resistance

ABSTRACT

Fe-based protective coatings are promising alternatives to replace large or expensive mechanical structures in aggressive environments, such as, in petrochemical industries. In this work, we have evaluated the corrosion and abrasive wear resistance of coatings produced by the HVOF thermal spray process using the commercial SAF2507 Superduplex alloy modified by the addition of 3.0 wt% boron. Three coatings were obtained from different metal powders produced by different routes (spray forming and high energy ball milling). The coatings had a partially amorphous structure containing a dispersion of nanocrystalline borides, such as Fe_3B and $(Fe,Cr)_2B$. The coatings showed significant improvement in abrasive wear resistance and preserved the high corrosion resistance of the commercial SAF2507 Superduplex alloy.

1. Introduction

The good properties, such as high corrosion and wear resistance associated with Fe-based bulk metallic glasses (BMGs) have attracted large scientific and technological interest in recent years. Numerous papers [1–14] have discussed how to use these alloys to take advantage of their good properties.

Amorphous and/or nanocrystalline structures are often required to achieve good corrosion and wear resistance such as those found in BMGs alloys, and therefore, the use of non-conventional processes involving high cooling rates of the molten metal [15] is necessary. Among the most prominent techniques, we can highlight the thermal spray technique called high velocity oxygen fuel (HVOF).

HVOF is widely used in the industry to protect structures from aggressive environments [16]. Compared with flame and plasma spray, the HVOF coatings exhibit low porosity, high hardness, high adhesion as a result of the high particle velocity at impact and a relatively low particle temperature process [17]. The technique can replace the expensive cobalt and nickel-based alloys and the conventional hard chrome electrodeposition process. Some benefits of HVOF process compared with the hard chrome electrodeposition process are the low capital investment, the low energy cost, the range of materials choice, the waste disposal are not toxic, no limitation on size of part, the high deposition rates, the equipment can be portable and fewer process steps [18].

Some disadvantages of HVOF process include the parameters model and the system control, because of its inherent complexity. The amount of heat content in the HVOF system is very high, so over heating of the substrate is quite likely. Difficult to coat inside diameters, the layer uniformity, the deposition control and the surface finish are some disadvantages of the HVOF process compared with electrodeposition process, for example [18].

Several works [3–5,7–10] have reported the advantages of using HVOF dense protective coatings for their excellent corrosion properties. The corrosion current densities are typically on the order of 10^{-5} and 10^{-6} A/cm^2 in potentiodynamic polarization tests in saline solution. Some reports [6,11,12] have also revealed the superior wear resistance. But few works [13–14] have reported the influence of microstructure on both, corrosion and wear resistance.

The alloy composition plays an important role in corrosion and wear resistance. Z. Zhou et al. [3] call the attention for the importance of the addition of beneficial alloying elements for the improvement of corrosion properties. In some cases, the alloy composition is more important

* Corresponding author at: Rod. Washington Luiz km. 235, 13565–905 São Carlos, SP, P.O. Box 60, Brazil.
E-mail address: berger.edu@gmail.com (J.E. Berger).

http://dx.doi.org/10.1016/j.surfcoat.2016.10.062
0257-8972/

for corrosion resistance than having an amorphous structure. Botta et al. [1] also confirmed the important role of Cr for the corrosion properties of amorphous Fe-based alloys, and report excellent corrosion properties for the system FeCrNiB in neutral, acid or alkaline solutions containing chloride ions.

The high corrosion resistance of amorphous alloys is related to the homogeneous chemical structure and the absence of crystallographic imperfections, such as, grains, grain boundaries, second phase elements, dislocations and segregations [19,20]. The passive film formed on the surface of these materials is more uniform and stable than the films formed on the surface of crystalline alloys [1].

In terms of abrasion wear resistance, the use of boron as alloying element to promote the formation of borides in microstructures has been reported to be beneficial. The presence of B to form continuous three-dimensional networks of borides, has been reported to improve the material protection against abrasive particles present in aggressive environments. Zepon et al. [2] reported the formation of $(Fe,Cr)_2B$ in Fe-based alloys by spray forming. The abrasive wear resistance measured by dry sand against rubber wheel is better at high volume fraction of borides and for small boride inter-particle distance.

In the present work, the influence of different powders used in the HVOF process on the microstructure, corrosion and abrasive wear resistance of coatings made using commercial SAF2507 Superduplex alloy with additions of boron was studied. The commercial SAF2507 Superduplex alloy was used because of its close chemical composition to an amorphous FeCrNiB alloy studied in a previous work [1] which presented excellent corrosion resistance properties. We used the denomination SDM (Superduplex modified) in the present study to refer to this alloy composition. The coating was characterized by X-ray diffraction (XRD), differential scanning calorimetry (DSC), scanning electron microscopy (SEM) and transmission electron microscopy (TEM). The corrosion properties were evaluated by potentiodynamic polarization in saline media and the abrasive wear resistance was evaluated by the standardized dry sand/rubber wheel test (ASTM G65-04).

2. Materials and methods

The selected alloy composition in this studied was the commercial SAF2507 Superduplex alloy modified by the addition of 3.0 wt% of boron using a Fe-B alloy. The compositions of both alloys are listed in Table 1. The addition of commercially pure elements such as Cr and Ni was also made to adjust the alloy composition. The final composition is listed in Table 1 and called SDM (Superduplex modified).

Amorphous ribbons were prepared using an ingot made by arc-melting. The induction-melting was performed under a high purity argon atmosphere in a quartz tube. The ingot was injected through a nozzle onto a Cu wheel, rotating at 1500 rpm, to produce rapidly solidified ribbons by melt spinning. The ribbons had a thickness of about 10 μm and width of 1.5 mm. The amorphous ribbons were characterized by X-ray diffraction (XRD) and differential scanning calorimetry (DSC).

Three different powders were produced for the HVOF thermal spray process. The powders were first produced by a spray forming process using the parameters shown in Table 2. The overspray powder with the particle size <45 μm composed the first powder, and was called: powder (Spray). The overspray powder with the particle size >45 μm was subjected to a high energy ball milling process in a ZOZ mill using the parameters listed in Table 3. After milling, two powders were obtained: the first one with a particle size smaller than 45 μm, called: powder (ZOZ-1) and the second one with a particle size between 20 and 53 μm, called powder (ZOZ-2).

Table 1
Composition of commercial SAF2507 Superduplex, Fe-B and SDM alloys.

Alloy	Chemical composition (wt.%)										
	C	Si	Mn	Cr	Ni	Mo	P	S	N	B	Fe
SAF 2507	0.027	0.50	0.97	24.1	7.13	3.58	0.031	0.006	0.3	–	Bal
Fe-B	0.3	0.57	–	–	–	–	–	–	–	16.5	Bal
SDM	0.12	0.23	1.83	21.40	6.68	1.31	0.010	0.005	0.3	3.06	Bal

Table 2
Parameters used in the spray forming process.

Parameter	Process 1	Process 2	Process 3
Gas flow – N_2 [m^3/min]	3.84	3.84	3.84
Mass flow [kg/min]	6,66	4.85	4.50
Gas-to-metal ratio [m^3/kg]	0.58	0.79	0.85
Pouring temperature [°C]	1700	1700	1700
Total powder mass [g]	738	618	981
Powder mass with particle size <45 μm [g]	290		
Powder mass with particle size >45 μm [g]	2047		

The three different powders were thermally sprayed by HVOF on an API 5L × 80 alloy substrate. This steel is used as riser pipes in oil extraction processes. The parameters used for the HVOF thermal spray are shown in Table 4. The three different coatings are called SDM HVOF (Spray), SDM HVOF (ZOZ-1) and SDM HVOF (ZOZ-2), referring to the respective powders used.

The samples were characterized structurally by XRD using a Rigaku diffractometer, model Geigerflex ME210GF2 with Cu-Kα radiation (λ = 1,5418 Å); by DSC in a Netzsch 404 equipment with a heating rate of 40 °C/min; by MET/EDS using Philips CM120 microscope with an accelerating voltage of 120 kV and a FEI Tecnai G2 microscope with an accelerating voltage of 200 kV and by SEM/EDS using a microscope Stereoscan 440 - LEO which was attached an EDS analyzer - 250 Inca - Oxford.

The corrosion resistance properties were evaluated from the polarization curves in a salty environment (35 g/L NaCl) using a potentiostat/galvanostat PGSTAT Metrohm Model 302N AUTOLAB BV, the counter electrode used was platinum and the reference electrode was a silver chloride electrode (Ag/AgCl). Open-circuit tests were conducted for 30 min and the potentiodynamic analysis started at a potential 100 mV below the equilibrium potential in open-circuit until the current density reached a value of 1 or 0.1 mA/cm^2. The scanning speed was 1 mV/s. The surface finish of all samples was the same using 1 μm diamond paste. The data of the polarization curves were obtained by the NOVA 1.10 software and the corrosion current density was obtained by the Tafel extrapolation method. The good reproducibility was ensured by repeating each test thrice.

The wear resistance of the coatings was evaluated by abrasive wear tests on rubber wheel and dry sand, following the ASTM G65-04. Procedure B was adopted from the standard which involves wheel speed of 200 rpm for 10 min.

3. Results and discussion

The structural analysis of the ribbon obtained by the melt-spinning process is shown in Fig. 1. The ribbon shows a diffuse X-rays diffraction

Table 3
Parameters used in the high energy ball milling process.

Parameter	Values
Ball mass [g]	12,000
Powder mass (45–250 μm) [g]	400
Ball-to-powder ratio	30:1
Ball diameter [mm]	5.0
Milling rotation speed [rpm]	650
Milling time [h]	8
Discharging rotation speed [rpm]	250
Discharging time [h]	24

Table 4
HVOF parameters used for all samples.

Parameters	Values
Fuel flow (kerosene) [m^3/s]	5.36×10^{-6}
O_2 flow [m^3/s]	0.875
Carrier flow at 0.34 MPa [m^3/s]	9.43×10^{-3}
Barrel length [m]	0.10
Combustion pressure [MPa]	0.63
O_2 back pressure [MPa]	0.88
Fuel back pressure [MPa]	0.68
Stand off distance [m]	0.33
Wheel (powder feed rate) [rpm]	6.8
Step size [m]	0.01
Speed [mm/s]	0.5
# of passes	5

pattern typical of amorphous phases. The DSC thermogram shows two exothermic reactions indicating a crystallization onset temperature around 550 °C. No crystallite is seen on the TEM bright field image and a diffuse diffraction pattern is observed. All analyzes indicate an amorphous structure for the SDM alloy ribbon.

Fig. 2 shows the morphology of the powders used in the HVOF thermal spray process. The powder obtained directly from overspray shows a spherical shape and the surface is partially covered by a dendritic structure which indicates the partial formation of crystalline phases. The powders processed by high energy ball milling have a very irregular aspect due to the successive deformation, cold welding and fragmentation, inherent to the milling process [21].

Fig. 3 shows cross sections of coatings obtained from the different powders. It is found that all coatings are relatively well-bonded to substrates. The typical morphology of thermal spraying coatings is observed in all samples, which present pores, oxide inclusions and lamellar microstructures due to successive passes from the HVOF gun. A better particle size distribution (20–53 μm), in the powder SDM (ZOZ-2), provided lower porosity as seen in Table 5. Li and Christofides [17] explain that the powder size distribution is an important factor in thermal spray processes. A narrow particle size distribution leads to a more uniform and dense layer with low porosity.

The X-ray diffraction patterns of the coatings (Figs. 4, 5 and 6) indicate the formation of ferrite and austenite phases, typical in duplex steels and also the formation of two borides, one with tetrahedral structure (Fe_3B) and the other with an orthorhombic structure $(Fe,Cr)_2B$. Some oxides of the type $(Fe,Ni)_3O_4$ were observed in the SDM HVOF (ZOZ-1) coating probably because of the fine particle size used in this particular case (large surface to volume ratio).

The DSC thermograms of the coatings (Figs. 4, 5 and 6) show the presence of exothermic peaks indicating presence of amorphous phase which crystallize. The difference between the reactions stages and its temperatures are due to the formation of crystalline phases on spraying and therefore, the composition of amorphous phase in coatings is different from that of the fully amorphous ribbons (Fig. 1).

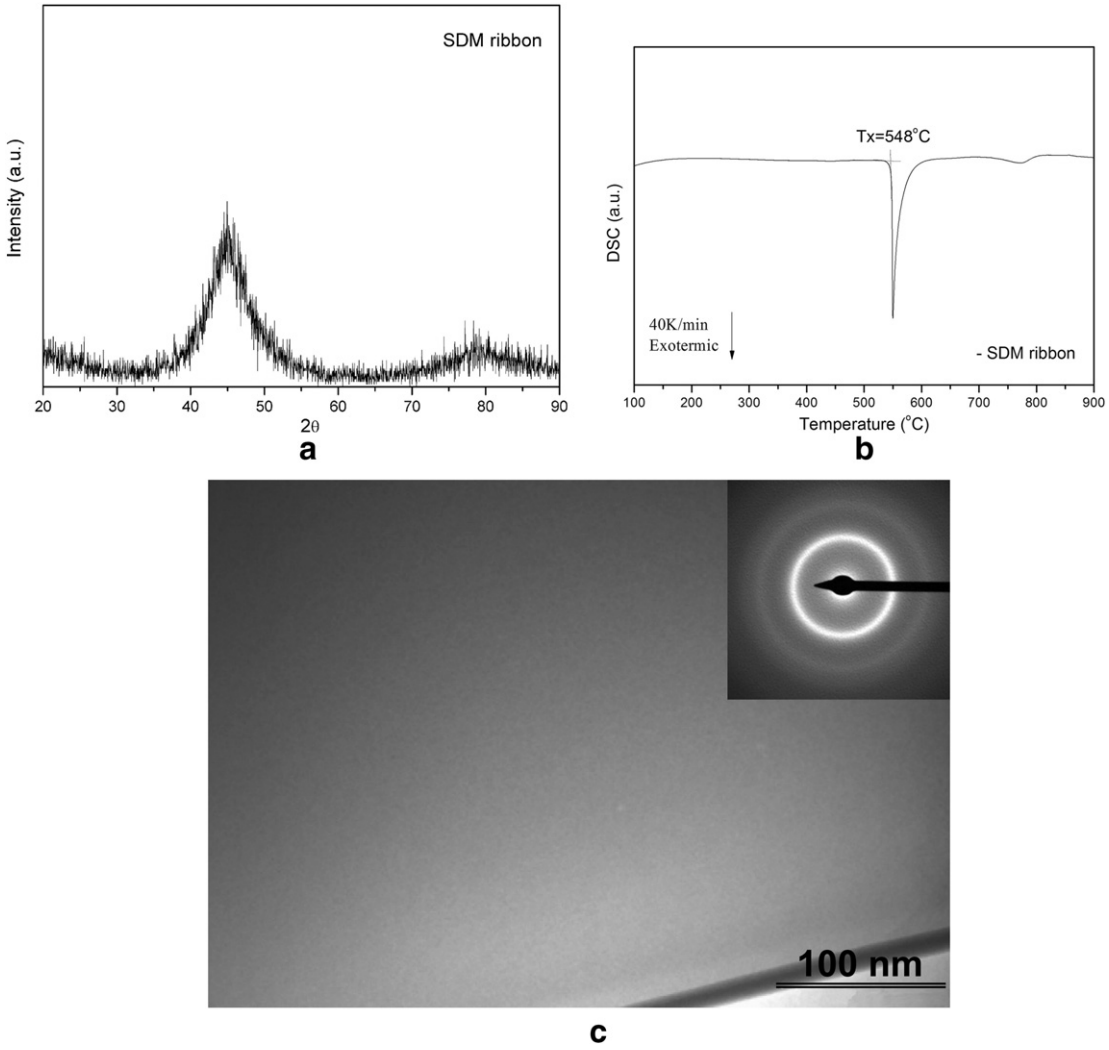

Fig. 1. Structural analysis of the SDM ribbon: (a) XRD pattern, (b) DSC thermogram and (c) Bright field TEM image with the respective electron diffraction pattern.

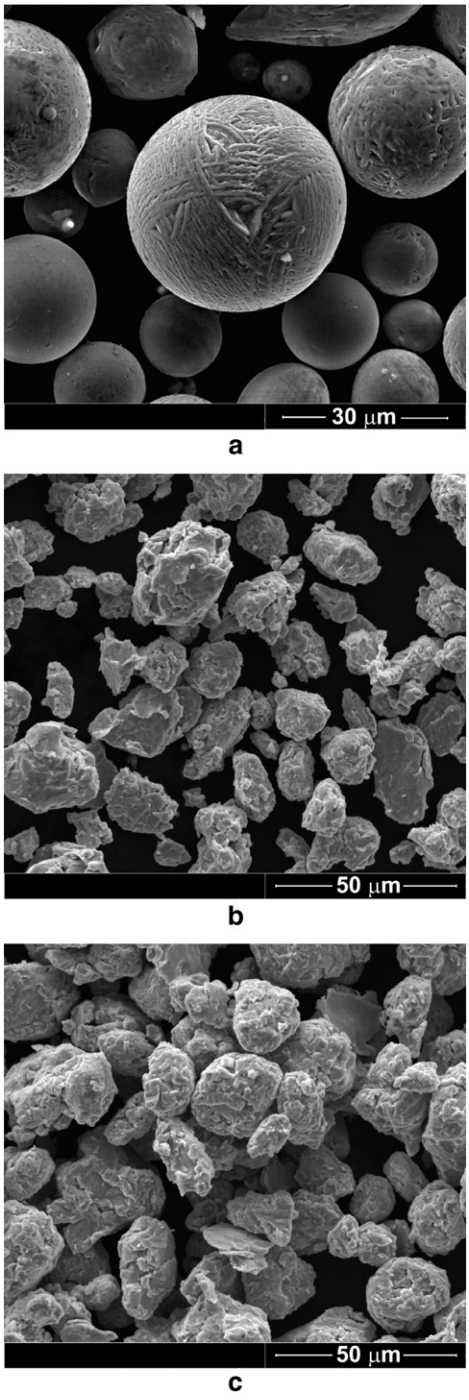

Fig. 2. Morphology of the powders used in the HVOF thermal spray process: (a) Powder SDM (Spray) <45 μm. (b) Powder SDM (ZOZ-1) <45 μm. (c) Powder SDM (ZOZ-2) 20–53 μm.

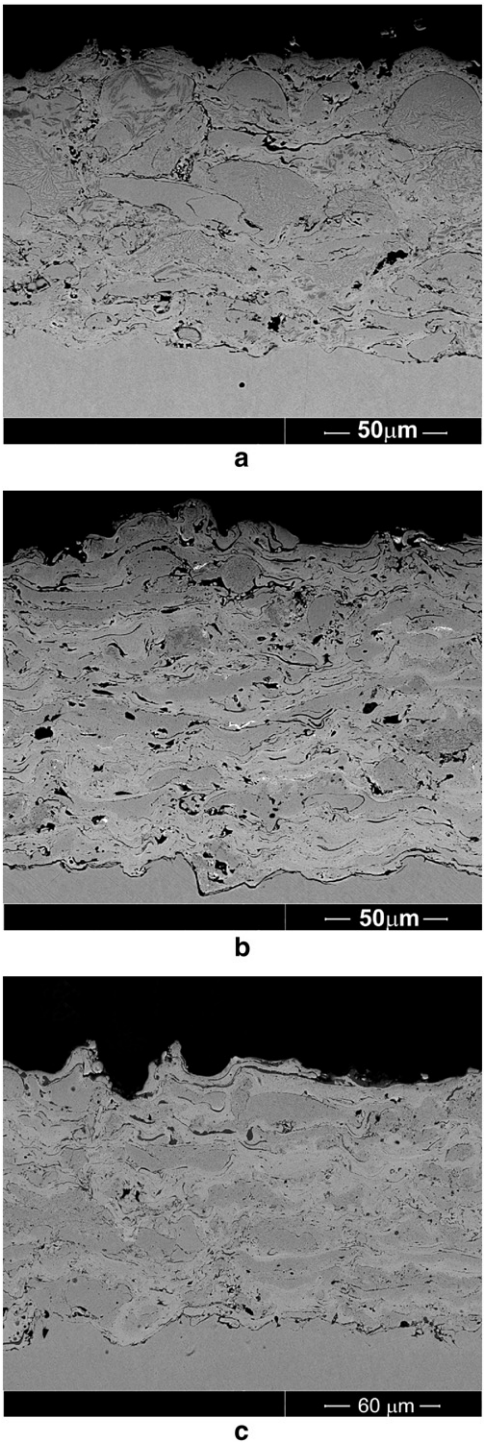

Fig. 3. Cross section of the three coatings obtained from the HVOF thermal spray process: (a) SDM HVOF (Spray). (b) SDM HVOF (ZOZ-1). (c) SDM HVOF (ZOZ-2).

Using the ratio between the area of the exothermic peaks of the coatings and the area of the exothermic peak of the amorphous ribbon, it was possible to evaluate the volume fraction of the amorphous phases in each coating. The percentages were approximately 30% for SDM HVOF (Spray) coating, 60% for SDM HVOF (ZOZ-1) coating and 40% for SDM HVOF (ZOZ-2) coating. It is observed that the highest percentage of amorphous phase was obtained in the SDM HVOF (ZOZ-1) coating obtained from the fine ball milled particles.

This coating shows the highest level of oxide and therefore, the large fraction of amorphous phase may be related to a higher level of oxygen

Table 5
Average thickness and porosity of the three coating layers obtained from the HVOF thermal spray process. Standard deviations in parenthesis.

	Average thickness [μm]	Porosity [%]
SDM HVOF (Spray) coating	112 (9)	2.9 (0.6)
SDM HVOF (ZOZ-1) coating	135 (10)	3.7 (0.5)
SDM HVOF (ZOZ-2) coating	103 (8)	0.51 (0.12)

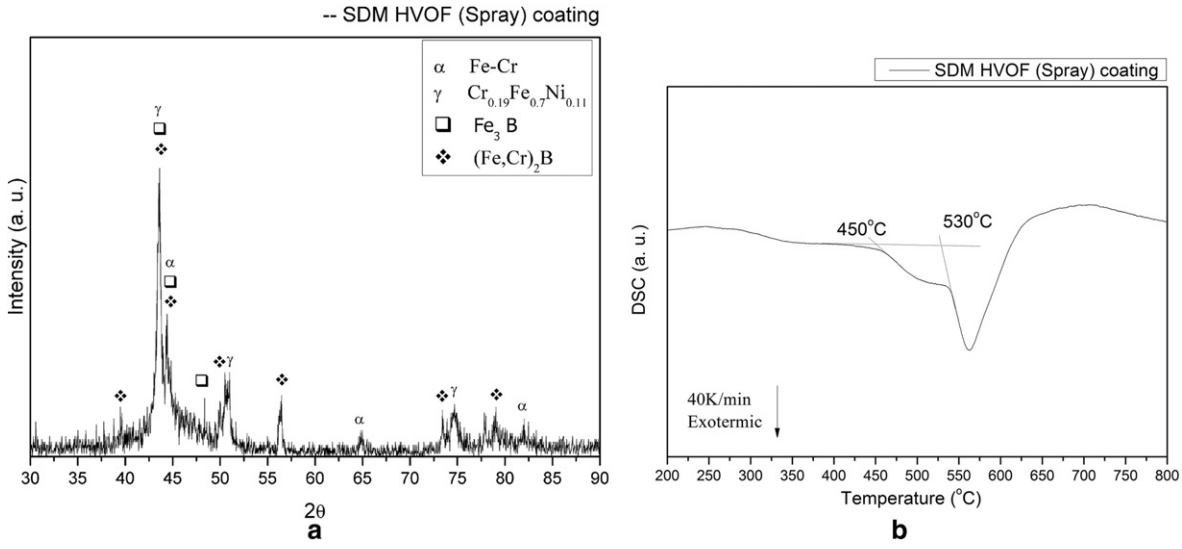

Fig. 4. (a) XRD pattern and (b) DSC thermogram of SDM HVOF (Spray) coating.

in this material. However, the properties of HVOF thermal spray coatings depends on several parameters such as particle velocity, particle size, temperature, oxidation, composition and so on, therefore complete understanding requires more investigation of the system [17].

Fig. 7 shows TEM bright field micrograph of the SDM HVOF (ZOZ-1) coating with clear suggestion that the HVOF processing was able to produce a predominantly amorphous layer.

Fig. 8(a) shows round features which were associated with the porosity from the HVOF processing and primary crystals from the solidification of the liquid with sizes in the range of 10–100 nm. Fig. 8(b) shows in greater details, again in a STEM dark field micrograph, the morphology and nucleation aspects associated with the crystals. New crystals are clearly nucleating either by direct contact with the existing crystals or in the regions nearby.

Fig. 9 shows a TEM picture of one of the largest crystal, and corresponding selected area electron diffraction pattern (SAEDP) which included the crystal and the surrounding matrix. The SAEDP clearly indicates an amorphous halo corresponding to the matrix and crystalline pattern which was indexed as the $(Fe,Cr)_2B$ tetragonal phase. This type of crystallite is often observed in these coatings, and they are easily identified by the typical fringes in their structure which indicate the presence of stacking faults. These features are typical of borides with M_2B structures [22]. EDS microanalysis of the crystallite (Table 6) showed the presence of Fe and Cr but no Ni. Boron is not detectable by this technique.

Fig. 10 shows the volume loss after five abrasive wear tests on rubber wheel and dry sand for the coatings, commercial SAF2507 Superduplex alloy and API 5L ×80 alloy. The average standard deviation is small for all samples. The Rockwell C hardness was inserted together in the graphic.

The three coatings show a higher hardness and a lower volumetric loss than the commercial SAF 2507 Superduplex and API 5L ×80 alloys. The wear resistance is about four times better for the HVOF coatings. Similar results were found by Fu et al. [23], which produced partially amorphous Fe-based coatings with excellent abrasive wear resistance, about 6 times higher than the comparative sample (arc-sprayed 3Cr13 coating), however, the effect of percentages of crystalline and amorphous phases on the coatings' wear resistance was not obvious.

Fig. 11 shows the SEM images of the worn surfaces of the three coatings. In this sort of wear test, the abrasive sand particles roll between the

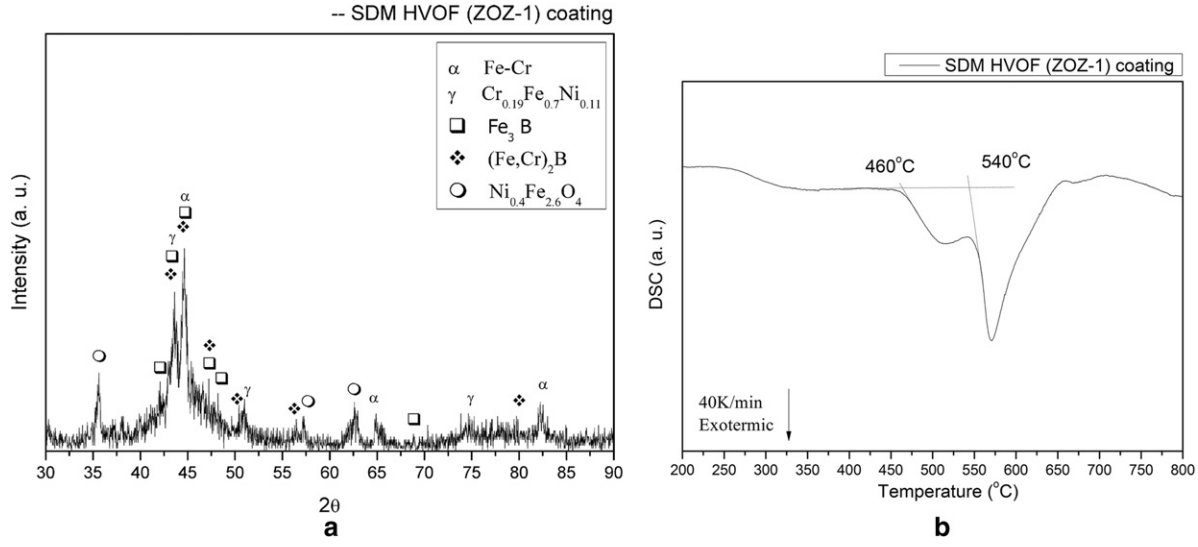

Fig. 5. (a) XRD pattern and (b) DSC thermogram of SDM HVOF (ZOZ-1) coating.

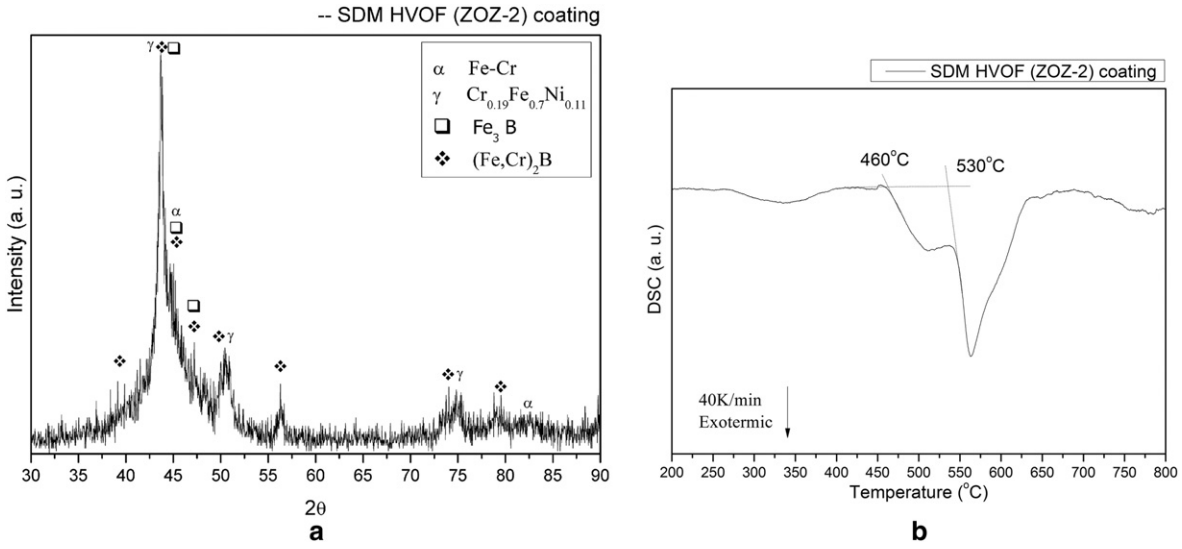

Fig. 6. (a) XRD pattern and (b) DSC thermogram of SDM HVOF (ZOZ-2) coating.

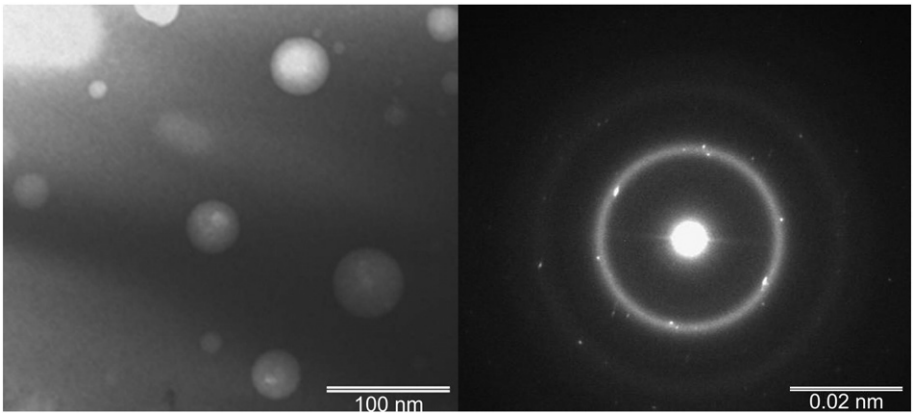

Fig. 7. TEM-BF micrograph showing area with small porosity and some crystallization of the SDM HVOF (ZOZ-1) coating.

rubber and sample surfaces, removing the surface material due to deep indentation and entrainment of the abrasive particles, forming the parallel grooves and scratches to the sliding direction seen in the images.

By observing Fig. 11, one can see a significant difference in the scratches concentration of the three coatings, which suggest the protection effect of borides nanocrystals in the coatings structure. The SDM

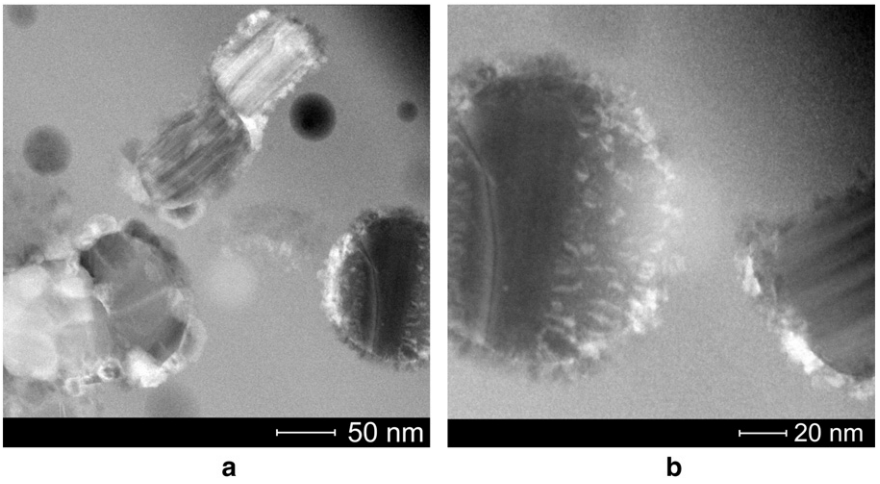

Fig. 8. STEM dark field micrographs of the HVOF coating with predominance of amorphous phase in (a) and detailed aspects of morphology and nucleation of the crystals forming in (b).

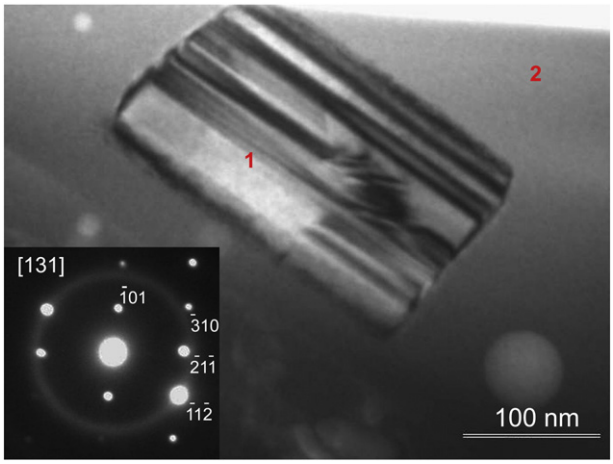

Fig. 9. Images in bright field and crystallite diffraction pattern for SDM HVOF (ZOZ-1) coating.

Table 6
Semi-quantitative EDS analysis performed in the regions indicated in Fig. 9.

Region	EDS analysis (wt.%)			
	Fe	Si	Cr	Ni
1 - Crystallite	56.04	1.94	42.01	0.00
2 - Matrix	70.35	1.01	17.39	11.23

HVOF (Spray) coating, the one with the highest percentage of crystalline structure, showed a low concentration of scratches, Fig. 11a, indicating an excellent abrasive wear resistance, as proved in the result of abrasive wear test in the Fig. 10, with the smallest volumetric loss. However the SDM HVOF (ZOZ-1) coating, Fig. 11b, the one with the lowest percentage of crystalline structure, showed a high concentration of scratches and the biggest volumetric loss among the coatings. Therefore, the presence of a higher amount of borides ensured a better performance in front of the abrasive wear mechanisms.

Fig. 12 show the polarization curves performed on the three SDM coatings, on commercial SAF2507 Superduplex alloy, on API 5L ×80 alloy and on the SDM amorphous ribbon. Table 7 show the main information obtained from the polarization curves; corrosion potential (Ecorr), corrosion current (icorr), critical potential (Ecrit), passivation width (ΔE = Ecrit − Ecorr) and corrosion rate. The values of Ecrit can be associated either with the disruption of the passive layer or with oxygen evolution. The critical potential or the breaking-off of the passive

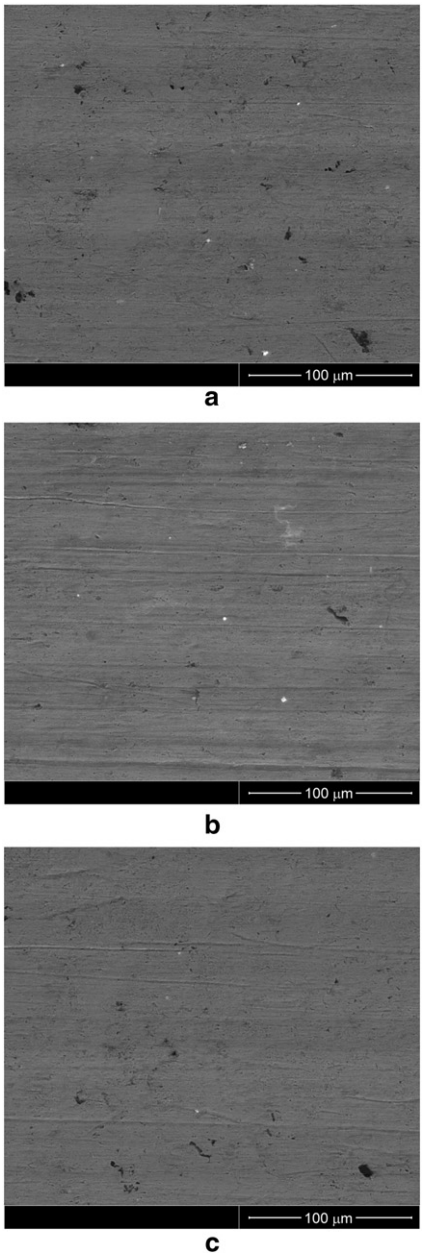

Fig. 11. SEM images (secondary electrons) of the worn surfaces of: (a) SDM HVOF (Spray) coating, (b) SDM HVOF (ZOZ-1) coating and (c) SDM HVOF (ZOZ-2) after the dry sand against rubber wheel abrasive wear test.

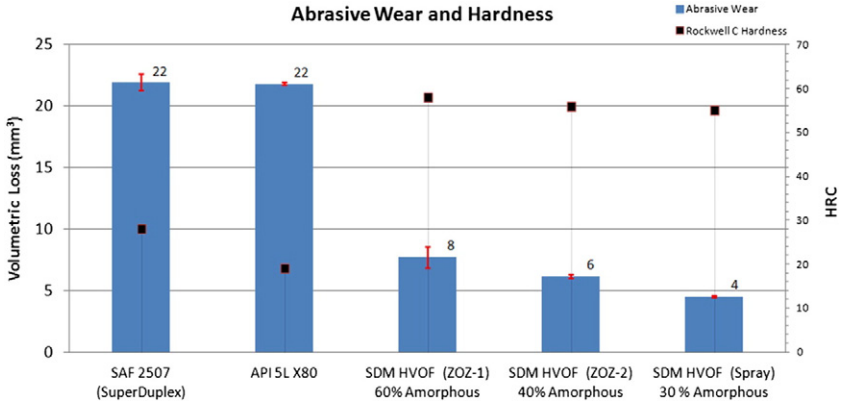

Fig. 10. Result of abrasive wear testing and hardness of the coatings and SAF2507, API 5L ×80 alloys.

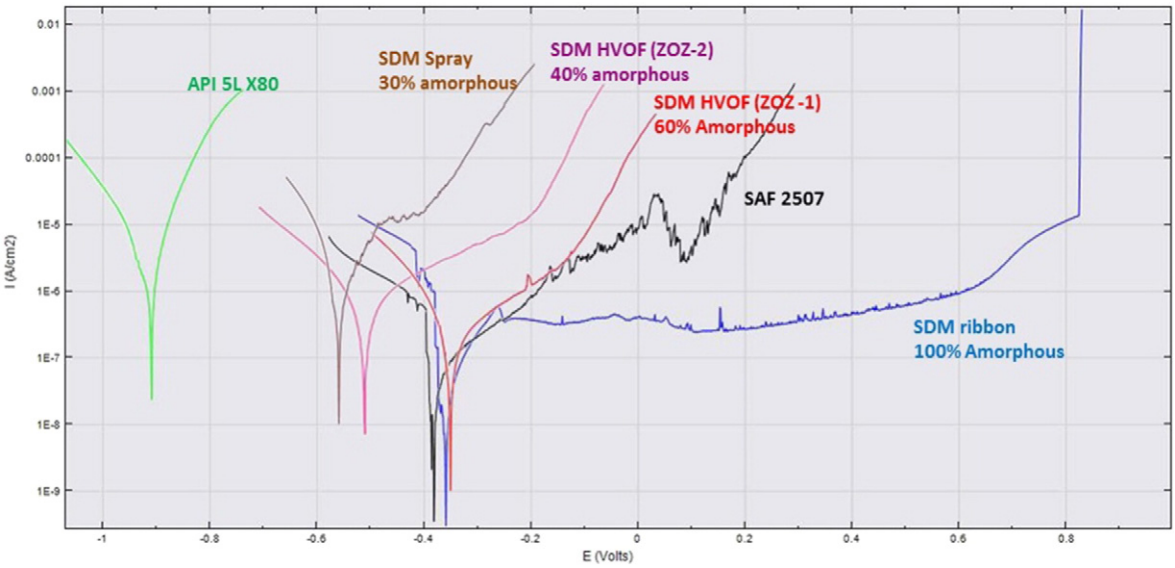

Fig. 12. Polarization curves of SDM HVOF coatings, SAF 2507 alloy, API 5L ×80 alloy and SDM amorphous ribbon. Neutral media with 35 g/L NaCl. Reference electrode: silver chloride (Ag/AgCl).

layer was defined as the potential where the current density reaches the level of 10 μA/cm^2.

As also noticed in previous work [1], the amorphous ribbon shows low corrosion current density and an extended stable passivation plateau. Low corrosion current density was also observed in commercial SAF2507 Superduplex alloy but no stable passivation plateau was detected.

For the SDM coatings, the higher the percentages of amorphous phase, the better the corrosion resistance. This trend can also be seen in the study [5], which produced partially amorphous Fe-based coatings by HVOF process, the coatings showed in the potentiodynamic polarization test, in saline solution, a corrosion current density in the order of 10^{-6} A/cm^2, with better results for the coatings with higher percentage of amorphous phase. According to Zhang et al. [5], the differences in corrosion resistance are due to the combined effect of oxidation and porosity in coatings.

The best performance is observed for the SDM HVOF (ZOZ-1) coating which has a slightly larger thickness compared to the other coatings. Generally, the corrosion properties of amorphous coatings are sensitive to the alloy composition and improve with lower porosity or higher amorphous phase content [3,24]. It is important to notice that the increase of corrosion resistance is gradual and not abrupt. Therefore, a good balance between corrosion and wear resistance can be made.

Indeed, a significant and important result can be seen for that SDM HVOF (ZOZ-1) coating which has the highest percentage of amorphous phase (60%). This sample shows a near corrosion current density, in the order of 10^{-7} A/cm^2, and similar corrosion potential to the SDM amorphous ribbon and the commercial SAF2507 Superduplex alloy, moreover, as seen before, an excellent wear resistance due to the presence of boride nanocrystals.

Finally API 5L ×80 alloy which has the worst corrosion resistance properties showed a corrosion current density on the order of 10^{-6} A/cm^2. It is worth noting that the corrosion current densities of these samples are relatively low. A corrosion current density of 10^{-5} A/cm^2 is equivalent to a corrosion rate of about 0.1 mm/year which is considered relatively small.

4. Conclusion

Three successful coatings were produced by HVOF thermal spray process from different SDM alloy powders. A narrow particle size distribution leads to a lower porosity level. Structural characterization showed a partially amorphous structure and a dispersion of nanocrystalline borides of the types Fe_3B and $(Fe,Cr)_2B$.

The SDM alloy showed a good glass forming ability during the HVOF thermal spray process, and proved to be a suitable alloy to protect steels in aggressive environments. The presence of nanocrystalline borides ensured a significant increase in abrasive wear resistance compared to commercial SAF 2507 Superduplex alloy without deterioration of the high corrosion resistance of this alloy.

Acknowledgements

The authors acknowledge the support of Hydro-Quebec Research Institute, Department of Materials Engineering at Federal University of São Carlos and the financial support of FAPESP (thematic project, grant number 2013/05987-8), CNPq and CAPES.

Table 7
Electrochemical properties obtained from the polarization curves of the SDM HVOF coatings, SAF 2507 alloy, API 5L ×80 alloy and SDM amorphous ribbon. Neutral media with 35 g/L NaCl. Reference electrode: silver chloride (Ag/AgCl).

	E_{corr} [mV]	E_{crit} [mV]	ΔE [mV]	I_{corr} [A/cm^2]	Corrosion rate [mm/year]
SDM amorphous ribbon	−358	785	1143	3×10^{-8}	3×10^{-4}
SAF 2507	−380	7	387	8×10^{-8}	9×10^{-4}
SDM HVOF (ZOZ-1) 60% amorfo	−350	−85	265	2×10^{-7}	2×10^{-3}
SDM HVOF (ZOZ-2) 40% amorfo	−505	−228	277	8×10^{-7}	9×10^{-3}
SDM HVOF (Spray) 30% amorfo	−548	−483	65	1×10^{-6}	1×10^{-2}
API 5L ×80	−910	−880	30	5×10^{-6}	5×10^{-2}

References

[1] W.J. Botta, J.E. Berger, C.S. Kiminami, V. Roche, R.P. Nogueira, C. Bolfarini, Corrosion resistance of Fe-based amorphous alloys, J. Alloys Compd. 586 (2014) S105–S110.

[2] G. Zepon, A.R.C. Nascimento, A.H. Kasama, R.P. Nogueira, C.S. Kiminami, W.J. Botta, C. Bolfarini, Design of wear resistant boron-modified supermartensitic stainless steel by spray forming process, Mater. Des. 83 (2015) 214–223.

[3] Z. Zhou, L. Wang, F.C. Wang, H.F. Zhang, Y.B. Liu, S.H. Xu, Formation and corrosion behavior of Fe-based amorphous metallic coatings by HVOF thermal spraying, Surf. Coat. Technol. 204 (2009) 563–570.

[4] R.Q. Guo, C. Zhang, Q. Chen, Y. Yang, N. Li, L. Liu, Study of structure and corrosion resistance of Fe-based amorphous coatings prepared by HVAF and HVOF, Corros. Sci. 53 (2011) 2351–2356.

[5] C. Zhang, R.Q. Guo, Y. Yang, Y. Wu, L. Liu, Influence of the size of spraying powders on the microstructure and corrosion resistance of Fe-based amorphous coating, Electrochim. Acta 56 (2011) 6380–6388.

[6] C. Zhang, L. Liu, K.C. Chan, Q. Chen, C.Y. Tang, Wear behavior of HVOF-sprayed Fe-based amorphous coatings, Intermetallics 29 (2012) 80–85.

[7] M.S. Bakare, K.T. Voisey, K. Chokethawai, D.G. McCartney, Corrosion behaviour of crystalline and amorphous forms of the glass forming alloy $Fe_{43}Cr_{16}Mo_{16}C_{15}B_{10}$, J. Alloys Compd. 527 (2012) 210–218.

[8] C. Cui, F. Ye, G. Song, Laser surface remelting of Fe-based alloy coatings deposited by HVOF, Surf. Coat. Technol. 206 (2012) 2388–2395.

[9] S.-L. Wang, J.-C. Cheng, S.-H. YI, L.-M. Ke, Corrosion resistance of Fe-based amorphous metallic matrix coating fabricated by HVOF thermal spraying, Trans. Nonferrous Metals Soc. China 24 (2014) 146–151.

[10] Y.-J. Qin, Y.-P. Wu, J.-F. Zhang, W.-M. Guo, S. Hong, L.-Y. Chen, Long-term corrosion behavior of HVOF sprayed FeCrSiBMn amorphous/nanocrystalline coating, Trans. Nonferrous Metals Soc. China 25 (2015) 1144–1150.

[11] G. Bolelli, T. Börner, A. Milanti, L. Lusvarghi, J. Laurila, H. Koivuluoto, K. Niemi, P. Vuoristo, Tribological behavior of HVOF- and HVAF- sprayed composite coatings based on Fe-Alloy + WC–12% Co, Surf. Coat. Technol. 248 (2014) 104–112.

[12] W. Wang, C. Zhang, P. Xu, M. Yasir, L. Liu, Enhancement of oxidation and wear resistance of Fe-based amorphous coatings by surface modification of feedstock powders, Mater. Des. 73 (2015) 35–41.

[13] H.S. Ni, X.H. Liu, X.C. Chang, W.L. Hou, W. Liu, J.Q. Wang, High performance amorphous steel coating prepared by HVOF thermal spraying, J. Alloys Compd. 467 (2009) 163–167.

[14] W.-H. Liu, F.-S. Shieu, W.-T. Hsiao, Enhancement of wear and corrosion resistance of iron-based hard coatings deposited by high-velocity oxygen fuel (HVOF) thermal spraying, Surf. Coat. Technol. 249 (2014) 24–41.

[15] W.H. Wang, C. Dong, C.H. Shek, Bulk metallic glasses, Mater. Sci. Eng. R 44 (2004) 45–89.

[16] N. Cinca, J.M. Guilemany, Thermal spraying of transition metal aluminides: an overview, Intermetallics 24 (2012) 60–72.

[17] M. Li, P.D. Christofides, Modeling and control of high-velocity oxygen-fuel (HVOF) thermal spray: a tutorial review, J. Term. Spray Technol. 18 (2009) 753–768.

[18] Azom, Thermal spraying versus hard chrome plating, Mater. Aust. 32–6 (2000) 11–13.

[19] M. Naka, K. Hashimoto, T. Masumoto, Corrosion resistivity of amorphous iron alloys containing chromium, J. Jpn. Inst. Metals 38 (1974) 835–841.

[20] K.E. Heusler, D. Huerta, Proc. Symp. on corrosion, electrochemistry and catalysis of metallic glasses, in: R.B. Diegle, K. Hashimoto (Eds.), The Electrochem, Soc, Pennington, USA 1988, p. 261.

[21] C. SURYANARAYANA, Mechanical alloying and milling, Prog. Mater. Sci. 46 (2001) 1–184.

[22] Y.-J. Lin, J. Hu, Borides in microcrystalline Fe-Cr-Mo-B-Si alloys, J. Mater. Sci. 26 (1991) 2833–2840.

[23] B.-Y. Fu, D.-Y. He, L.-D. Zhao, Effect of heat treatment on the microstructure and mechanical properties of Fe-based amorphous coatings, J. Alloys Compd. 480 (2009) 422–427.

[24] A.P. Wang, C. Chang, W.L. Shou, J.Q. Wang, Preparation and corrosion behavior of amorphous Ni-based alloy coatings, Mater. Sci. Eng. A 449–451 (2007) 277–280.